Motion Determination in Space-Time Images

Bernd Jähne
Physical Oceanography Research Division A-030, Scripps Institution of Oceanography
La Jolla, CA 92093, USA
and
Institut für Umweltphysik, Universität Heidelberg, Im Neuenheimer Feld 366
D-6900 Heidelberg, Federal Republik of Germany

Abstract

A new approach to determine motion from multiple images of a sequence is presented. Motion is regarded as orientation in a three-dimensional space with one time and two space coordinates. The algorithm is analogous to an eigenvalue analysis of the inertia tensor. Besides the determination of the displacement vector field it allows the classification of four regions with regard to motion: a) constant regions, where no velocity determination is possible; b) edges, where the velocity component perpendicular to the edge is determined; c) corners, where both components of the velocity vector are calculated; d) motion discontinuities, which are used to mark the boundaries between objects moving with different velocities.

The accuracy of the new algorithm has been tested with artificially generated image sequences with known velocity vector fields. An iterative refinement technique yields more accurate results than the usage of higher order approximations to the first spatial and temporal derivatives. Temporal smoothing significantly improves the velocity estimates in noisy images. Displacements between consecutive images can be computed with an accuracy well below 0.1 pixel distances.

1 Introduction

Classical image sequence processing analyses motion from only two consecutive images of a sequence [16,17,18]. Since digital image processing hardware has become powerful enough to store, process, and display image sequences with many frames, considerable efforts have been made to extend these approaches to the simultaneous analysis of many images or the whole sequence. *Heeger* [6] used a set of similar but differently oriented space-time quadrature filter to determine the displacement vector field. A least square method is applied to compute the two-dimensional displacement vector field from the set of filter responses. In a similar approach, *Fleet and Jepson* [4] decompose an image sequence by a family of spatiotemporal velocity-tuned linear filters, but they calculate the velocity component normal to the filtered spatial orientation from local phase information. In a second step, the normal displacements are combined to gain the two-dimensional displacement vector.

Common to both approaches is the usage a large sets of velocity-tuned filters. It arises the question whether it is not possible to calculate the displacement more directly.

In this paper, a technique is discussed which originates from an analysis of the local orientation in the three-dimensional image sequence space with one time and two space coordinates. Such an approach to motion analysis has a long history in biological vision [1], but the developments presented here have rather been triggered by a complex physical

application for image sequence processing, the analysis of the motions of small scale waves on a water surface [9,10,8,12].

In the first section of the paper the concept of motion determination by analysis of orientation is outlined and it is shown that determining the local orientation in the $\boldsymbol{xt}$-space is equivalent to the eigenvalue analysis of the inertia tensor.

The rest of the paper is committed to the important issue of the accuracy of the velocity determination. Basically, three classes of errors can be distinguished:

- errors inherent to the algorithms used to compute the displacement vector field;
- errors caused by the imaging sensor such as signal noise, nonuniformity of the sensor elements, and geometrical distortions;
- errors due to the fact that the optical flow on the image plane and the two-dimensional motion field which is the perspective projection of the three-dimensional motion field in the observed scene are not identical. In a recent paper, *Verri and Poggio* [21] nicely demonstrate that both are in general different. *Nagel* [19] discusses additional terms to be included in the constraint equations for optical flow.

This paper deals only with the first class of errors. To separate algorithm related errors from sensor related errors, only computed image sequences have been used.

2 Motion and Orientation in xt-Space

2.1 The Concept

As an introduction to the concept, let us take an object $g(\boldsymbol{x})$ in the image sequence which moves with constant speed $\boldsymbol{u}$. In this case it can be described by

$$g(\boldsymbol{x}, t) = g(\boldsymbol{x} - \boldsymbol{u}t) \tag{1}$$

This equation is known as the general solution of the differential equation for waves in a non-dispersive medium in physics. The usage of the three-dimensional space with one time and two space coordinates offers the advantage that motion can also be analyzed in the corresponding Fourier space which will be denoted by $\boldsymbol{k}\omega$-space. Correspondingly, the abbreviation $\boldsymbol{xt}$-space will be used.

An object moving with a constant velocity has a simple representation in the $\boldsymbol{k}\omega$-space. Fourier transformation of (1) gives

$$\hat{g}(\boldsymbol{k}, \omega) = \hat{g}(\boldsymbol{k})\, \delta(\boldsymbol{k}\boldsymbol{u} - \omega) \tag{2}$$

where δ is the Dirac distribution. With constant motion only one plane in the $\boldsymbol{k}\omega$-space is occupied by the wavenumber spectrum $\hat{g}(\boldsymbol{k})$ of the object which is given by

$$\omega = \boldsymbol{k}\boldsymbol{u} \tag{3}$$

This plane intersects the $k_1 k_2$-plane perpendicularly to the direction of the motion, because in this direction the scalar product $\boldsymbol{k}\boldsymbol{u}$ vanishes. The slope of the plane is proportional to the velocity.

The plane cannot be determined unambiguously if the wavenumber spectra lies on a line. In this case, the spatial structure of the object is oriented only in one direction (local spatial orientation respectively edge-like structure). Then only the velocity component

perpendicularly to the edge can be determined. This problem is the well known *aperture problem* [16,7].

So far, the considerations have been limited to continuous $\boldsymbol{x}t$- and $\boldsymbol{k}\omega$-spaces. Yet all conclusions remain valid for discrete image sequences if the sampling theorem is satisfied. Then the image sequence can be exactly reconstructed from its samples. For image sequences there is a sampling condition both for the space and time coordinates [7] which requires that both the highest frequencies and wavenumbers are sampled at least twice per period and wavelength respectively.

2.2 The Analogy: Eigenvalue Analysis of the Inertia Tensor

In the previous section it has been discussed that motion and orientation analysis are equivalent. Therefore algorithms for orientation can also be used for motion analysis. One approach uses a set of directional quadrature filter pairs [14]. All filters show the same shape but only differ in the direction they select. Combining the filter outputs in a suitable way gives an estimate of the orientation. Such a procedure has been implemented by Heeger [6] for two-dimensional motion analysis using a set of $\boldsymbol{x}t$-Gabor filters.

A more direct way has recently be presented by *Bigün and Granlund* [2]. They point out that the determination of local orientation in a multidimensional space is equivalent to a line fit through the origin in Fourier space. Local orientation in a neighborhood corresponds to the mathematical term of *linear symmetry* defined by

$$g(\boldsymbol{x}) = g(\boldsymbol{x}\boldsymbol{k}_0) \tag{4}$$

where $\boldsymbol{k}_0$ denotes the orientation of the greyvalue structure. For the sake of simplicity time is regarded as one component of the $\boldsymbol{x}$-vector and the frequency ω as one component of the $\boldsymbol{k}$-vector. The greyvalue is constant in a plane perpendicular to $\boldsymbol{k}_0$. Thus linear symmetry is equivalent to a line in the Fourier space.

The analysis of the distribution of the spectral energy in the $\boldsymbol{k}\omega$-space can be performed by referring to a physical analogy. If we consider the spectral density as the density of a rotary body rotating about the axis $\boldsymbol{k}_0$, the inertia is given by

$$J = \int_{-\infty}^{\infty} d^2(\boldsymbol{k}, \boldsymbol{k}_0) |\hat{g}(\boldsymbol{k})|^2 \, \mathrm{d}\boldsymbol{k} \tag{5}$$

where d is the (Euclidian) distance function between the vector $\boldsymbol{k}$ and the line presented by $\boldsymbol{k}_0$.

Using this analogy, it will now be shown that an *eigenvalue analysis* of the inertia tensor will allow a motion analysis. The inertia tensor corresponding to the inertia defined by (5) has the following elements [5,2]

$$\begin{aligned} \text{diagonal elements} \quad & J_{ii} = \sum_{j \neq i} \int_{-\infty}^{\infty} k_j^2 |\hat{g}(\boldsymbol{k})|^2 \mathrm{d}\boldsymbol{k} \\ \text{nondiagonal elements} \quad & J_{ij} = -\int_{-\infty}^{\infty} k_i k_j |\hat{g}(\boldsymbol{k})|^2 \mathrm{d}\boldsymbol{k} \end{aligned} \tag{6}$$

Now let us consider different shapes of the spectral distribution:

- *Point at origin.* This corresponds to a region of constant greyvalues. The inertia is zero for rotation about all possible axes, consequently all eigenvalues of the inertia tensor are zero. No motion can be detected since no plane can be fitted through a point at the origin.
- *Line through origin.* In this case, a spatially oriented pattern is moving with constant speed. It is only possible to detect the velocity component perpendicularly to the spatial orientation. One eigenvalue of the inertia tensor is zero, since the rotation about the axis coinciding with the line has no inertia. The orientation of this line and thus the spatial orientation and the normal velocity are given by the eigenvector to the eigenvalue zero.
- *Plane trough origin.* This case corresponds to a region of constant motion with a spatially distributed pattern. Rotation about a axis normal to the plane has a maximum inertia, thus the eigenvector to the maximum eigenvalue gives the orientation of the plane and thus both components of the velocity.
- *Three-dimensional rotary body.* Now motion is no longer constant in the region.

2.3 Calculation of the inertia tensor in x*t*-space

The tensor elements (6) can readily be calculated in the $\boldsymbol{x}$-space since they contain scalar products of the form

$$k_j^2 |\hat{g}(\boldsymbol{k})|^2 = |\mathrm{i}k_j \hat{g}(\boldsymbol{k})|^2 \tag{7}$$

and

$$k_i k_j |\hat{g}(\boldsymbol{k})|^2 = \mathrm{i}k_i \hat{g}(\boldsymbol{k}) \; [\mathrm{i}k_j \hat{g}(\boldsymbol{k})]^* \tag{8}$$

where the superscript * denotes the conjugate complex. According to Parseval's theorem the integral (6) in $\boldsymbol{k}$-space can also be performed in the $\boldsymbol{x}$-space using the inverse Fourier transform of the corresponding expressions:

$$\begin{aligned} \text{diagonal elements} \quad J_{ii} &= \sum_{j \neq i} \int_{-\infty}^{\infty} \left(\frac{\partial g}{\partial x_j} \right)^2 \mathrm{d}\boldsymbol{x} \\ \text{nondiagonal elements} \quad J_{ij} &= -\int_{-\infty}^{\infty} \frac{\partial g}{\partial x_i} \frac{\partial g}{\partial x_j} \mathrm{d}\boldsymbol{x} \end{aligned} \tag{9}$$

Finally, a weighting function $w(\boldsymbol{x})$ is used to limit the determination of the inertia tensor to a certain local neighborhood in the image sequence:

$$\begin{aligned} \text{diagonal elements} \quad J_{ii}(\boldsymbol{x}_0) &= \sum_{j \neq i} \int_{-\infty}^{\infty} w(\boldsymbol{x} - \boldsymbol{x}_0) \left(\frac{\partial g}{\partial x_j} \right)^2 \mathrm{d}\boldsymbol{x} \\ \text{nondiagonal elements} \quad J_{ij}(\boldsymbol{x}_0) &= -\int_{-\infty}^{\infty} w(\boldsymbol{x} - \boldsymbol{x}_0) \frac{\partial g}{\partial x_i} \frac{\partial g}{\partial x_j} \mathrm{d}\boldsymbol{x} \end{aligned} \tag{10}$$

The width of the weighting function w determines the spatial resolution of the algorithm. In discrete images the operations contained in (10) can be performed as convolutions with appropriate operators and summarized in the operator expression

$$\begin{aligned} &\text{diagonal elements ii} \quad \sum_{j \neq i} \boldsymbol{B}(\boldsymbol{D}_j \bullet \boldsymbol{D}_j) \\ &\text{nondiagonal elements ij} \quad \boldsymbol{B}(\boldsymbol{D}_i \bullet \boldsymbol{D}_j) \end{aligned} \tag{11}$$

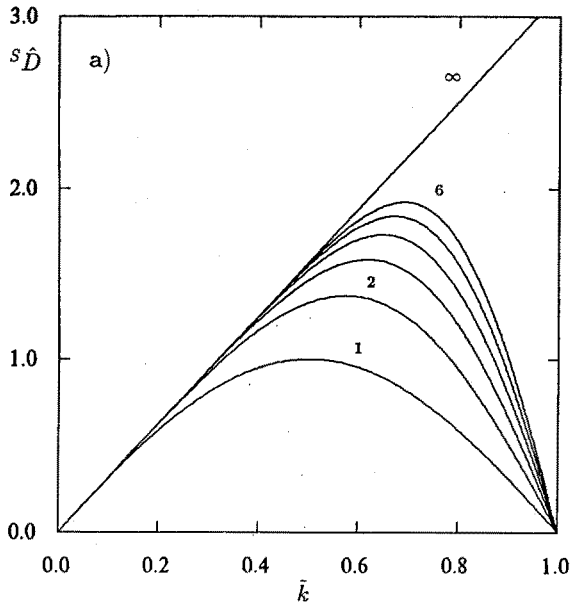

Fig. 1: Transfer function (imaginary part, the real part is zero) of the convolution masks (13) used to approximate the derivative operator. The straight line shows the transfer function of an ideal derivative operator.

The symbol $\boldsymbol{D}_i$ denotes a partial derivation with respect to the coordinate i, $\boldsymbol{B}$ a smoothing operator. Smoothing is performed over all coordinates. Finally, the symbol $\bullet$ denotes the pointwise multiplication of the filter results of the two derivations. This is a *nonlinear* operation which cannot be interchanged with the smoothing operation $\boldsymbol{B}$. In the following, the results of the operations (11) applied on the image sequence $\boldsymbol{G}$ will be abbreviated with the notation

$$G_{ij} = [\boldsymbol{B}(\boldsymbol{D}_i \bullet \boldsymbol{D}_j)]\boldsymbol{G} \tag{12}$$

Efficient algorithms for the eigenvalue and eigenvector analysis in two and three dimensions, i.e. for one- and two dimensional velocity determination, are discussed in another paper [11].

3 Error considerations

Kearney et al. [13] give a detailed analysis of the gradient-based optical flow determination. They point out that highly textures surfaces, i.e. just the region with steep gradients where the flow can be detected most easily are most seriously effected by errors because of larger higher order spatial derivatives. Actually, this is not correct. It can be proven that any region with constant motion (1) yields an accurate velocity estimate in the one- and two dimensional case.

The problem is rather the discrete approximation of the spatial and temporal derivatives. The simple 1/2(1 0 -1)-operator is a poor approximation for higher wavenumbers (Figure 1). Therefore higher order approximations have been used with the following

convolution masks [7]

$$\begin{aligned} {}^{(1)}\boldsymbol{D}_i &= 1/2(1\ 0\ -1) \\ {}^{(2)}\boldsymbol{D}_i &= 1/12(-1\ 8\ 0\ -8\ 1) \\ {}^{(3)}\boldsymbol{D}_i &= 1/60(1\ -9\ 45\ 0\ -45\ 9\ -1) \end{aligned} \tag{13}$$

The corresponding transfer functions in Figure 1 show that these masks approximate an ideal derivative operator better with increasing size of the mask, but even the largest mask shows considerable deviations for wavenumbers larger than 0.6 times the Nyquist wavenumber.

Because of this bad performance, also the idea of iterative refinement has been tested. The next determination is computed in a coordinate system which is moving with the previously estimated velocity. If the previous estimate has diminished the residual velocity, the temporal frequencies are smaller. Consequently, the temporal derivative will be calculated more accurately. It should be expected that the iteration finally converges to the correct solution provided a) the spatial interpolation necessary to calculate the temporal derivative is accurate enough and b) the image sequence includes no aliasing.

4 Experimental Results

4.1 Computed Image Sequences

The accuary of the algorithms has been tested with different computed image sequences. All experiments have been performed with 12-bit images. All convolutions and multiplications were computed in 16-bit integer arithmetic with appropriate scaling. All intermediate results were stored with 12-bit accuracy directly in a 12-bit frame buffer (FG-100 from Imaging Technology). Smoothing of the multiplications of the derivative operators in (11) was performed by a $17 \times 17 \times 5$ binomial kernel. Only the last steps of calculating the velocity components and the classification were performed in floating point arithmetic.

4.2 Accuracy: Dependence on spatial and temporal scales

The first set of experiments deals with the accuracy of the velocity estimate. Constantly moving sinusoidal patterns provided a means to test the influence of the wavenumber of the spatial structure on motion determination. To study subpixel accuracies non-integer values for the displacements and wavelengths have been used. Non-zero Gaussian noise with a standard deviation of 50 was added to the sinusoidal pattern with an amplitude of 500. A low displacement of only 0.137 pixels/frame was chosen to introduce no significant error in the temporal derivative. Figure 2a shows the computed displacement as a function of the wavelength using the three different approximations to the first derivative as discussed in section 3.

As expected, the deviations from the correct value increase with decreasing wavelength and are larger for lower order approximations. Towards larger wavelengths the estimated displacements converge to a value which deviates by less than 0.007 pixels from the correct value. This residual deviation is probably due to round-off errors caused by the 16-bit integer arithmetic and storage of intermediate results with only 12 bits accuracy. Taking this error limit, we can conclude that the first order approximation for the derivation

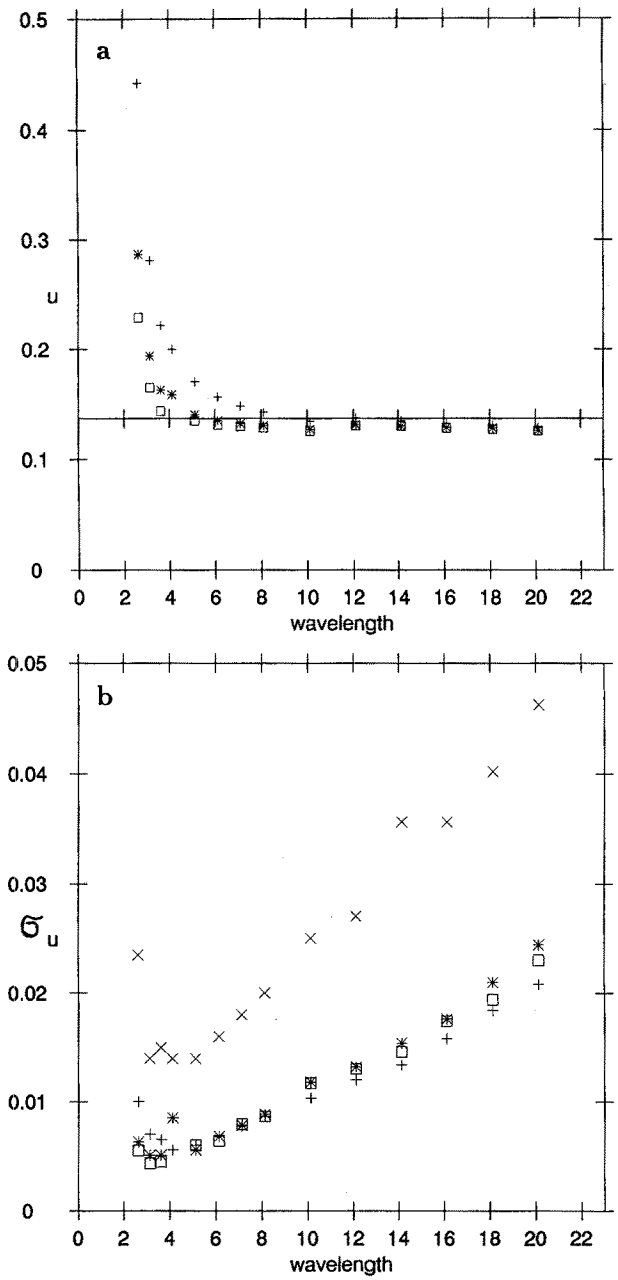

Fig. 2: a) Displacement estimate in an image sequence with a noisy sinusoidal pattern (amplitude 500, standard deviation of the Gaussian noise 50) moving with 0.137 pixels/frame as a function of the wavelength. Different discrete approximations for the first partial derivatives (13) have been used: $+$ ${}^{(1)}\boldsymbol{D}_i$, $*$ ${}^{(2)}\boldsymbol{D}_i$, $\square$ ${}^{(3)}\boldsymbol{D}_i$. b) standard deviation of the displacement distribution in the image as a function of the wavelength, symbols as in a) but an additional case with ${}^{(1)}\boldsymbol{D}_i$ where no temporal smoothing has been applied.

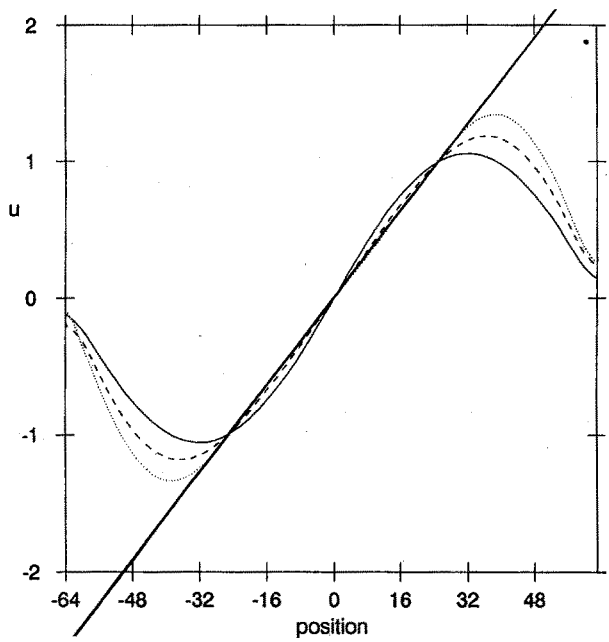

Fig. 3: A contracting sinusoidal pattern generates a linearly changing 1D-motion field. The contraction rate has been adjusted to result in displacements of half a wavelength at the left and right side of the image. The thick line marks the given velocity field, while the thin line show the computed results with different derivation operators (13): solid, 1/2(1 0 -1); dashed, 1/12 (-1 8 0 -8 1); dotted, 1/60 (1 -9 45 0 -45 9 -1). Wavelength of the pattern 5.10 pixels.

operator can be taken only if the wavelength is larger than 8 pixels, while the third order approximation yields about the same error at wavelengths as short as 3.5 pixels. This is still a factor of about two short to the smallest wavelength allowed by the sampling theorem with a wavelength of two pixels.

A linearly changing velocity nicely demonstrates the combined errors caused by both the spatial and temporal derivates. Since the displacement changes from $-\lambda/2$ to $\lambda/2$ over the image, just the frequencies are covered which are allowed by the sampling theorem. With low displacements, the error is dominated by the spatial derivative (Figure 3). The estimated displacements are too high and decrease with the order of approximation. For high displacements the error is dominated by the temporal derivative. Towards displacements of half a wavelength, the estimates even decrease and go towards zero. The computed behavior excellently agree with the expected one since it just resembles the transfer functions of the derivative operator shown in Figure 1. Interestingly, there is one point were the estimates are correct though both derivates are erroneous. This happens with a displacement of one pixel since then the temporal and spatial derivative are equal. Thus it has to be taken great care not to use integer displacements to test the accuracy of motion determination.

So far, there is the limitation that both the spatial and temporal frequencies must be well below the Nyquist limit. To overcome this problem the accuracy and convergence of the iterative refinement technique discussed in section 3 have been investigated. A 1/2 (1

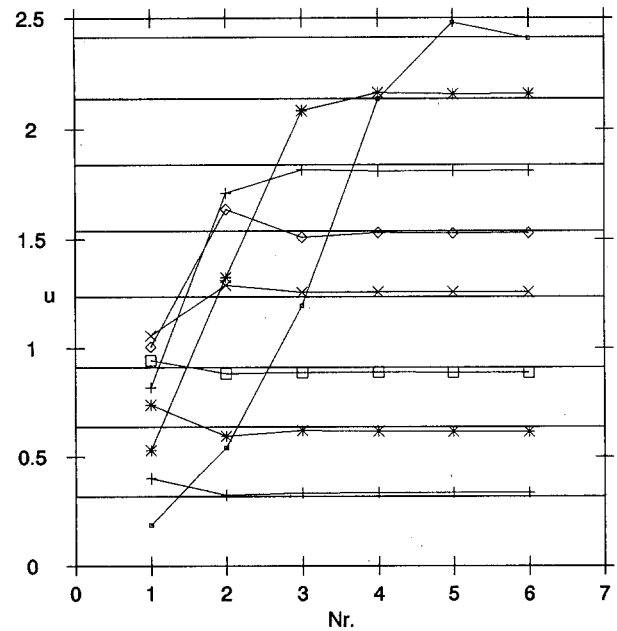

Fig. 4: Test of the method of iterative refinement with a sinusoidal pattern of a wavelength of 5.13 pixels. The computed displacements are shown as a function of the number of iterations for velocities between 0.317 and 2.413 pixels/frame. The thick lines mark the correct values.

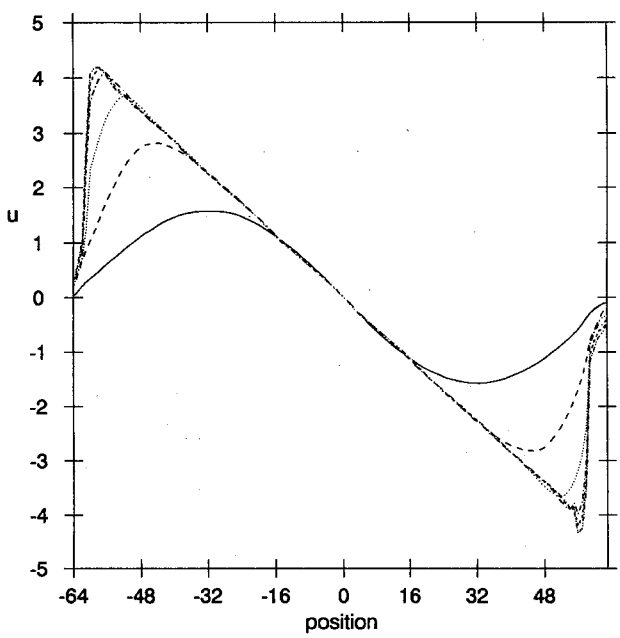

Fig. 5: Same as Figure 3 but displacements computed iteratively using the simple 1/2(1 0 -1) derivation operator. The iteration steps are indicated. Amplitude of the pattern 800; standard deviation of added zero mean Gaussian noise: 50.

σ_n	u	σ_u	u	σ_u	u	σ_u
	$\lambda = 4.13$		$\lambda = 6.13$		$\lambda = 8.13$	
10	0.1520	0.0017	0.1142	0.0021	0.1004	0.0027
20	0.1521	0.0027	0.1142	0.0032	0.1000	0.0041
50	0.1523	0.0058	0.1143	0.0067	0.1001	0.0087
100	0.1521	0.0116	0.1138	0.0135	0.1000	0.0174
200	0.1706	0.0321	0.1231	0.0354	0.1064	0.0430

TABLE 1: Dependence of the standard deviation of the displacement estimate σ_u on the standard deviation of the added Gaussian noise σ_n for a sinusoidal pattern of an amplitude of 500, moving with 0.1 pixels/frame.

0 -1) derivative operator and linear interpolation to estimate intergrid image points were applied. Despite the relative crude estimates in each step, the results are surprisingly good. Figures 4 and 5 show that the algorithm converges nearly in the whole possible displacement range of $\pm\lambda/2$. Of course the convergence is slower at higher displacements because the poor initial estimates allow only a slow decrease in the residual displacement but within 6 iterations the final values have been reached. The small deviations from the expected values are less than 0.03 pixels and obviously depend on the actual displacement.

4.3 Influence of Noise

The last section clearly showed that accurate estimates of the velocities can be computed. Now the standard deviation of the estimates is closer examined. First we take a look at the dependence of the standard deviation on the wavelength of the image structure at a constant noise level. Then standard deviation basically is proportional to the wavelength (Figure 2b). This fact results from the decrease of the spatial derivative with the wavelength. Only at small wavelengths were the estimate becomes erroneous (Figure 2a), it increases again.

In a second experiment the noise level was increased in a sequence with a sinusoidal pattern of 4.13 pixel wavelength, an amplitude of 500 and a displacement of 0.137 pixels/frame. Table 1 shows that standard deviation of the velocity estimate σ_u is roughly proportional to the noise level σ_n. Only at the highest noise level, with almost a signal-to-noise ratio of one, the increase is more than proportional and the estimate is biased, but well within the standard deviation. The fact that the bias is larger at smaller wavelength clearly indicates that it is caused by the local nonlinearity in the transfer function of the partial derivative which is larger at higher wavenumbers (Figure 1).

The robustness of the estimate using the iterative refinement technique in noisy images with linearly changing velocity field is demonstrated in Figure 5b.

4.4 Moving random pattern

So far rather unrealistic images with periodical patterns have been studied which helped to understand the dependence of the errors on various parameters. In contrast, a moving random pattern (Figure 6a) includes spatial scales of all sizes and should thus give a good estimate of the errors in real images.

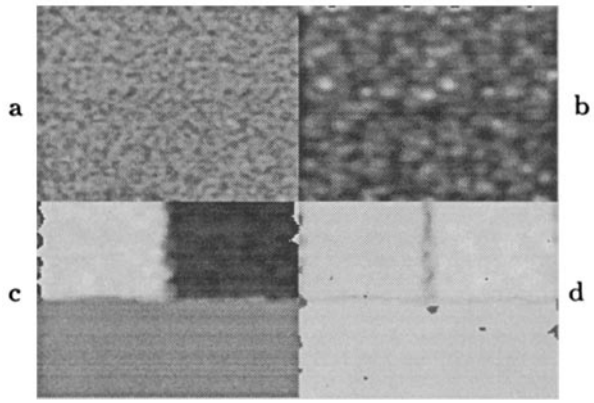

Fig. 6: Detection of motion discontinuities: a) One image of a sequence with random pattern which is moving 0.5 pixels/frame to the left and right in the upper left and right quadrants respectively. The lower half is not moving. b) Confidence level for motion detection. c) Computed 1D-velocity shown on a greyscale where zero velocity indicates a mean greyvalue. d) Measure indicating the degree of constant motion.

technique	u	σ_u
first order appr.	-0.555	0.015
second order appr.	-0.516	0.012
third order appr.	-0.501	0.019
iterative refinement	-0.494	0.020

TABLE 2: Displacement estimates for a random pattern ($\sigma_p = 362$) moving with -0.5 pixels/frame and $\sigma_n = 50$) using different techniques: different orders of approximation for the discrete partial derivatives or the iterative refinement technique.

Figure 6 shows several parameters. The sum of the squared derivatives is taken as a confidence level whether a velocity can be determined at all. The quantity γ measures the degree of constant motion and nicely shows the motion discontinuities (Figure 6c, d).

Table 2 shows that quite similar results as with the sinusoidal patterns are gained. The estimates get better for higher order approximations of the discrete derivatives. For the third order and the iterative refinement technique, the estimates agree within the standard deviation with the correct values. Despite the quite low signal-to-noise ratio of 7.2, the standard deviation is between 0.012 and 0.020 pixels. These values are three to four times higher than in comparable signal-to-noise ratios for sinusoidal pattern.

There is an easy explanation for this effect. In contrast to the sinusoidal pattern, the random pattern includes many regions with lower confidence levels for velocity estimates (Figure 6b). This measure averaged over the whole image is about four times lower for the random pattern than for the sinusoidal pattern. The noise sensitivity should be accordingly higher and this is exactly what has been observed. Thus the random pattern should give a realistic estimate of the influence of noise on the statistical error of the velocity estimate.

5 Conclusions

A new algorithm has been outlined for the analysis of motion in image sequences in the xt-space. Several tests performed with the 1D-algorithm indicate that a promising new approach to image sequence analysis opens up which is especially suitable for scientific and industrial applications. Accurate velocity determinations are possible even with noisy images. The algorithm proved to be superior to the standard optical flow approach using only two consecutive images of a sequence. The method of iterative refinements gives the most accurate results, which no detectable bias within the statistical error.

The algorithm is best used in a multigrid approach. The experiments demonstrated that the statistical errors are minimal for wavelengths between 3 to 6 pixel (Figure 2b). Therefore the image sequence may be spatially decomposed into a Laplacian pyramid [3,7] which is constructed in such a way that the maximum of the transfer function in each level coincides with the optimum wavenumber. In this way, also velocity information can also be gained from large scale structures, which otherwise would be lost. If no motion superimpostion is present, large displacements can be determined in a coarse-to-fine strategy.

Acknowledgements

The author gratefully acknowledges financial support by the German Science Foundation, the European Community (twinning contract with several Dutch organizations within the VIERS-1 project), the California Space Institute, and the Office of Naval Research.

References

1. E. H. Adelson, J. R. Bergen, Spatio-temporal energy models for the perception of motion, *J. Opt. Soc. America*, A2, 284–299 (1985).
2. J. Bigün, G. H. Granlund, Optimal orientation detection of linear symmetry, In *Proc. Int. Conference Computer Vision, London 1987*, , ed., pp. 433–438, IEEE Computer Society Press, Washington (1987).
3. P. J. Burt, E. H. Adelson, The Laplacian pyramid as a compact image code, *IEEE Trans. Comm.*, 31, 532–540 (1983).
4. D. J. Fleet, A. D. Jepson, Hierarchical construction of orientation and velocity selective filters, *IEEE Trans. Pattern Analysis and Machine Intelligence*, 11, 315–325 (1989).
5. H. Goldstein, *Klassische Mechanik*, Aula, Wiesbaden (1985).
6. D. J. Heeger, Optical flow using spatiotemporal filters, *Int. J. Comp. Vision*, 1, 279–302 (1988).
7. B. Jähne, *Digitale Bildverarbeitung*, Springer, Berlin, Heidelberg (1989).
8. B. Jähne, Energy balance in small-scale waves — an experimental approach using optical slope measuring technique and image processing, In *Radar scattering from modulated wind waves*, G. Komen, W. Oost, eds., pp. 105–120, Reidel, Dordrecht (1989).
9. B. Jähne, Image sequence analysis in environmental physics: water surface waves and air-sea gas exchange (in German), In *Mustererkennung 1986, Proc. 8. DAGM-Symposium, Paderborn*, G. Hartmann, ed., pp. 201–205, Springer, Berlin (1986).
10. B. Jähne, Image sequence analysis of complex physical objects: nonlinear small scale water surface waves, In *Proc. Int. Conference Computer Vision, London 1987*, pp. 191–200, IEEE Computer Society Press, Washington (1987).

11. B. Jähne, Motion determination in Space-Time Images, In *Image Processing III*, Conf. Proceedings 1135, SPIE, Washington (1989 in press).
12. B. Jähne, S. Waas, Optical measuring technique for small scale water surface waves, In *Advanced Optical Instrumentation for Remote Sensing of the Earth's Surface*, Conf. Proceedings 1129, SPIE, Washington (1989 in press).
13. J. K. Kearney, W. B. Thompson, D. L. Boley, Optical flow estimation: an error analysis of gradient based methods with local optimization, *IEEE Trans. Pattern Analysis and Machine Intelligence*, 9, 229–244 (1987).
14. H. Knutsson, *Filtering and reconstruction in image processing*, Dissertation, Linköping University (1982).
15. R. Lenz, Zur Genauigkeit der Videometrie mit CCD-Sensoren, In *Mustererkennung 1988, Proc. 10. DAGM-Symposium, Zürich*, pp. 179–189, Springer, Berlin (1988).
16. H. Nagel, Analyse und Interpretation von Bildfolgen I, *Informatik Spektrum*, 8, 178–200 (1985).
17. H. Nagel, Analyse und Interpretation von Bildfolgen II, *Informatik Spektrum*, 8, 312–327 (1985).
18. H. Nagel, Image sequences — ten (octal) years — from phenomenology towards a theoretical foundation, In *Proc. Int. Conf. Pattern Recognition, Paris 1986*, , ed., pp. 1174–1185, IEEE Computer Soc. Press, Washington (1986).
19. H. Nagel, On the constraint equation for the estimation of displacement rates in image sequences, *IEEE Trans. Pattern Analysis and Machine Intelligence*, 11, 13–30 (1989).
20. E. van Halsema, B. Jähne, W. A. Oost, C. Calkoen, P. Snoeij, First results of the VIERS-1 experiment, In *Radar scattering from modulated wind waves*, G. Komen, W. Oost, eds., p. , Reidel, Dordrecht (1989).
21. A. Verri, T. Poggio, Motion field and optical flow: qualitative properties, *IEEE Trans. Pattern Analysis and Machine Intelligence*, 11, 490–498 (1989).